Journal of Alloys and Compounds 902 (2022) 163759

Contents lists available at ScienceDirect

Journal of Alloys and Compounds

journal homepage: www.elsevier.com/locate/jalcom

Intricate magnetic behavior of Fe_6Ge_5 and its origin within a complex iron framework: The magnetic and ^{57}Fe Mössbauer study

Roman A. Khalaniya[a,*], Valeriy Yu. Verchenko[a,b], Alexey V. Sobolev[a], Igor A. Presniakov[a], Zheng Wei[c], Evgeny V. Dikarev[c], Andrei V. Shevelkov[a]

[a] Department of Chemistry, Lomonosov Moscow State University, 119991 Moscow, Russia
[b] National Institute of Chemical Physics and Biophysics, 12618 Tallinn, Estonia
[c] Department of Chemistry, University at Albany, Albany, New York 12222, United States

ARTICLE INFO

Article history:
Received 21 October 2021
Received in revised form 8 January 2022
Accepted 10 January 2022
Available online 12 January 2022

Keywords:
Intermetallics
Iron
Magnetically ordered materials
Crystal Growth
Mössbauer spectroscopy
Magnetic measurements

ABSTRACT

Fe_6Ge_5 was synthesized from the elements both as single crystals and a polycrystalline powder. Its crystal structure was reinvestigated in a wide temperature range using high-resolution powder and single-crystal X-ray diffraction. The crystal structure of Fe_6Ge_5 is connected with those of other iron germanides and features an alternation of iron-rich and germanium-rich layers. The magnetic behavior was studied by magnetization measurements on a single crystal and ^{57}Fe Mössbauer spectroscopy. The results of both methods showed that a peculiar two-step antiferromagnetic ordering (T_{N1} = 110 K, T_{N2} = 330 K) takes place, with the part of iron magnetic moments remaining disordered between the transitions. Such behavior originates from the large number of both symmetrically and locally distinct iron atoms that form a weakly connected iron framework and yield the competition between ferromagnetic and antiferromagnetic interactions.

© 2022 Elsevier B.V. All rights reserved.

1. Introduction

While in chemistry of ionic and covalent inorganic compounds basic rules of formation and structure-properties dependencies have been largely determined, for intermetallic compounds, which demonstrate more complex nature of chemical bonding, such interrelationships are still being established. In this regard, the study of regularities of how binary intermetallic compounds form and which physical properties they demonstrate is of great interest. Among such systems, we can specifically highlight the Fe-Ge system, which is one of the richest in the number of intermediate compounds [1,2]. In their crystal structures, it is possible to identify similar structural motifs with gradual evolution of coordination polyhedra of Ge atoms, and the compounds themselves exhibit a wide variety of physical properties [1]. While most compounds in the Fe-Ge system exhibit metallic conductivity typical for intermetallic compounds, the system also features an insulator, Fe_2Ge_3 [3]. Magnetic behavior in the Fe-Ge system is also represented by a wide spectrum ranging from simple ferromagnetism to various types of non-collinear antiferromagnetism [4–17].

As we noted in our previous work [1], physical properties of iron germanides are closely connected with the dimensionality of the iron atoms framework. While the iron-rich compounds with tightly bound 3-dimensional iron frameworks are predominantly ferromagnetic, the compounds with higher germanium content that feature low-dimensional fragments of iron atoms are antiferromagnetic due to Fe-Ge-Fe superexchange interactions or even non-metallic. Monoclinic FeGe and Fe_6Ge_5 feature iron frameworks composed of somewhat loosely connected low-dimensional fragments that can be considered as intermediate between those two cases. The former compound is an antiferromagnet that demonstrates complex temperature dependent magnetic behavior with two magnetic structures caused by the competition between ferromagnetic and antiferromagnetic interactions [1,12–15].

Fe_6Ge_5 possesses a crystal structure similar to that of monoclinic FeGe, yet with a larger number of iron sites as well as close Fe-Fe contacts, which might result in an even more intricate magnetic behavior. Despite the large number of works devoted to the study of binary iron germanides, Fe_6Ge_5 is still somewhat poorly characterized. Its crystal structure was examined in the literature by means of X-ray [18] and electron diffraction [19,20]; however, the crystal structure solution [18] contained large difference in the atomic displacement parameters of atomic sites. The reported results of its magnetization measurement also featured discrepancies due to

* Corresponding author.
E-mail address: khalaniya@inorg.chem.msu.ru (R.A. Khalaniya).

https://doi.org/10.1016/j.jallcom.2022.163759
0925-8388/© 2022 Elsevier B.V. All rights reserved.

possibly impure powder samples [21,22]. Fe_6Ge_5 occupies a special place at the border between known ferromagnetic and antiferromagnetic phases in the Fe-Ge system and its study could provide a deeper insight into peculiarities of magnetic interactions in iron germanides.

In this paper, we present a precise temperature-dependent structure determination of Fe_6Ge_5 and report on the magnetic and thermodynamic properties of this compound in a wide temperature range. We also present results of ^{57}Fe Mössbauer spectroscopy that provides a local picture of the atomic environment and magnetic structure. We discuss these features of Fe_6Ge_5 in comparison with other numerous compounds of the Fe-Ge system.

2. Experimental

2.1. Synthesis and characterization of powder samples

Synthesis of polycrystalline samples of Fe_6Ge_5 was carried out by the standard ampule technique. Fe powder (Sigma Aldrich, 99.99%) and Ge chips (Sigma Aldrich, 99.999%) were used as starting materials. The elements of a total mass of 0.5 g were weighed in the stoichiometric ratio of 6:5 and placed into a quartz ampule, which was then evacuated to the residual pressure of 10^{-3} Torr, sealed off, and annealed at 1000 °C for 2 days. After the first annealing, the specimen was ground and pressed into a pellet and then annealed again in a sealed and evacuated quartz ampule at 650 °C for 7 days. Phase composition of the obtained sample was investigated by powder X-ray diffraction using Cu $K\alpha_1$ radiation (Huber G670 diffractometer, λ = 1.5406 Å). Single crystals of Fe_6Ge_5 were obtained by a gas-phase chemical transport reaction using iodine as a transport agent. For this, the presynthesized Fe_6Ge_5 powder (0.1 g) was annealed with a small iodine crystal (5 mg) in a temperature gradient of 675–650 °C for 30 days in an evacuated quartz ampule.

2.2. Crystal structure determination of Fe_6Ge_5

Single-crystal X-ray diffraction experiments were performed using a Bruker D8 VENTURE diffractometer (Mo Kα, λ = 0.71073 Å). The crystal structure was solved by the Superflip program implemented in the Jana2006 package [23]. The Jana2006 software was also used for the subsequential refinement of the crystal structure. High-resolution X-ray powder diffraction experiments (HRPD) were performed at the ID22 beam line of the European Synchrotron Radiation Facility (ESRF, Grenoble, France, λ = 0.35451 Å) in the temperature range of 10–373 K. The crystal structure of Fe_6Ge_5 from these experiments was refined using the Rietveld method in the Jana2006 program.

Data collection and crystal structure parameters for Fe_6Ge_5 are given in Table 1. Atomic parameters and the most important interatomic distances are presented in Tables 2 and 3, respectively. Crystallographic information files for the single crystal and synchrotron powder data are deposited in the CCDC (ref. numbers 2116607–2116633) and available as a part of the Supplementary Material.

2.3. Magnetization and heat capacity measurements

Magnetization of the Fe_6Ge_5 single crystal was measured with the VSM setup of the Physical Property Measurement System (PPMS, Quantum Design) in external magnetic fields between 0.1 and 5 T in the temperature range from 2 to 380 K. Magnetization of several single crystals was measured with the VSM oven option operating in high vacuum (10^{-5} Torr) of the PPMS in external magnetic fields of 2 and 5 T in the temperature range of 300–900 K. Heat capacity measurements were performed on the Fe_6Ge_5 single crystal with the HC option using a relaxation-type calorimeter (PPMS, Quantum Design) in zero magnetic field between 2 and 125 K and between 300 and 340 K, and in 5 T field from 100 to 125 K.

Table 1
Crystallographic and refinement parameters for the Fe_6Ge_5 single crystal at T = 100 K. The crystal cell parameters were taken from the results of the synchrotron experiment at the same temperature.

refined composition	Fe_6Ge_5
molar weight	698.2 g mol^{-1}
structure type	Fe_6Ge_5
crystal system	Monoclinic
space group	*C*2/*m* (191)
a, Å	9.96973(4)
b, Å	7.82316(3)
c, Å	7.81275(3)
β, °	109.7968(2)
V, Å^3	573.341(4)
Z	4
d_{calc}, g/cm^3	8.0867
radiation/wavelength, Å	Mo Kα/0.71073
temperature, K	100
crystal form	elongated cuboid
crystal size, mm^3	0.06 × 0.03 × 0.03
absorption correction	Multi-scan
color	dark grey
θ range, °	3.39–43.12
range of *h, k, l*	− 19 ≤ h ≤ 15, − 15 ≤ k ≤ 15, − 14 ≤ l ≤ 15
number of parameters	61
number of reflections unique/measured	2228/4190
GoF	1.92
$\Delta\rho_{max}$ positive/negative, e/Å^3	4.91/− 5.43
$R[F^2 > 2\sigma(F^2)]$[a]/$R_w(F^2)$[b]	0.0454/0.0466

[a] $R(F) = \sum||F_o| - |F_c||/\sum|F_o|$.
[b] $R_w(F_o^2) = [\sum[w(F_o^2 - F_c^2)^2]/\sum wF_o^4]^{1/2}$; $w = 1/(\sigma^2(F) + 0.0001F^2)$.

Table 2
Atomic parameters for Fe_6Ge_5 single crystal at 100 K.

atom	site	*x*	*y*	*z*	U_{eq}, Å^2
Ge1	*4i*	0.36590(5)	0	0.00838(9)	0.00295(16)
Ge2	*8j*	0.04360(4)	0.19829(7)	0.21234(6)	0.00271(12)
Ge3	*4i*	0.34220(6)	0	0.37085(9)	0.00267(16)
Ge4	*4i*	0.14863(5)	0	0.59873(9)	0.00286(16)
Fe1	*8j*	0.28302(6)	0.26223(7)	0.17530(10)	0.00359(16)
Fe2	*4 f*	¼	¼	½	0.0023(2)
Fe3	*4 h*	0	0.25359(10)	½	0.0020(2)
Fe4	*4i*	0.12396(7)	0	0.01742(12)	0.0031(2)
Fe5	*4i*	0.58011(8)	0	0.28161(11)	0.0039(2)

2.4. Mössbauer spectroscopy

^{57}Fe Mössbauer spectra were recorded in a temperature range of 14–343 K in a closed-cycled SHI-850–1 JANIS cryostat using a conventional constant-acceleration spectrometer MS-1104Em in the transmission geometry. A radiation source ^{57}Co(Rh) was kept at room temperature. All isomer shifts are referred to α-Fe at 300 K. Experimental spectra were processed and analyzed using methods of spectral simulations implemented in the SpectrRelax program [24].

3. Results

3.1. Synthesis, crystal growth, and homogeneity range

Fe_6Ge_5 powder was obtained from the elements by a two-stage synthesis: annealing at 1000 °C, grinding and pressing into pellets, and second annealing at 650 °C. At the first stage, the initial mixture melts, and an ingot is obtained after cooling. The second stage yields the desired compound. Fe_6Ge_5 does not possess a noticeable homogeneity range; even small deviations from the Fe_6Ge_5 composition result in the presence of β-$Fe_{2-\delta}Ge$ or FeGe, depending on which of the elements was taken in excess.

Table 3
Selected interatomic distances for single crystal of Fe_6Ge_5 at 100 K.

Atom	Atom	Distance, Å
Ge1	Ge1	2.7210(12)
	Ge3	2.9204(11)
	Ge4	3.1999(9)
	Fe1 (×4)	2.5060(7) (×2)/2.7060(9) (×2)
	Fe4	2.4369(10)
	Fe5 (×2)	2.4555(9)/2.4998(12)
Ge2	Ge2 (×2)	3.1025(10)/3.1322(10)
	Ge3	3.2101(7)
	Ge4 (×2)	3.1897(8)/3.2364(8)
	Fe1 (×2)	2.5336(8)/2.5494(9)
	Fe2	2.5132(4)
	Fe3	2.4676(6)
	Fe4 (×2)	2.4887(10)/2.5275(7)
	Fe5	2.4214(5)
Ge3	Ge3	3.1099(11)
	Ge4	3.0367(11)
	Fe1 (×2)	2.5061(8)
	Fe2 (×2)	2.5133(5)
	Fe3 (×2)	2.4763(7)
	Fe4	2.8791(10)
	Fe5 (×2)	2.5589(11)/2.6893(12)
Ge4	Ge4	2.8401(9)
	Fe1 (×2)	2.4952(8)
	Fe2 (×2)	2.4433(5)
	Fe3 (×2)	2.4401(7)
	Fe5	2.5446(9)
Fe1	Fe1	2.5984(16)
	Fe2	2.6681(9)
	Fe3	2.7227(6)
	Fe4 (x2)	2.6306(7)/2.7446(11)
	Fe5	3.0627(11)/3.4649(9)
Fe2	Fe1 (×2)	2.6681(9)
	Fe3 (×2)	2.49260(3)
	Fe5 (×2)	2.7654(5)
Fe3	Fe5 (×2)	2.8612(9)
Fe4	Fe4	2.3932(15)

Single crystals of Fe_6Ge_5 were obtained by a chemical transport reaction in a temperature gradient of 675–650 °C, when a polycrystalline sample was annealed with addition of iodine as a transport agent. Large crystals of Fe_6Ge_5 up to several mm long could be obtained after one month of annealing.

3.2. Crystal structure of Fe_6Ge_5

X-ray diffraction analysis of the Fe_6Ge_5 single crystal obtained by the gas-phase chemical transport is generally consistent with the model reported in the literature [18]. According to our data, Fe_6Ge_5 crystallizes in its own structure type ($C2/m$, a = 9.96973(4) Å, b = 7.82316(3) Å, c = 7.81275(3) Å, β = 109.7968(2)°, Z = 4) and features a complex crystal structure composed of 9 crystallographically independent sites: 4 for germanium and 5 for iron. The crystal structure can be also represented as an alternation of iron-rich ribbons comprised of one- and two-capped $GeFe_{7/8}$ trigonal prisms and germanium-rich layers of isolated distorted Fe_2Ge_6 octahedra centered by Fe_2 dumbbells (Fig. 1).

While the crystal structure reported in the literature [18] featured large discrepancies between atomic displacement parameters of different sites, up to one order of magnitude, we observed much smaller deviations that do not exceed the factor of 2 both in the HRPD and single crystal data, which is expected for such a densely packed structure with large coordination numbers for all atoms (see Table 3). All nearest-neighbor distances (Table 3) are in a common range for Fe-Fe (> 2.5 Å), Ge-Ge (> 2.7 Å), and Fe-Ge (2.4–2.6 Å) contacts in other iron germanides [3,4,6,13,25,26] except the Fe4-Fe4 bond of 2.38 Å in the mentioned above Fe_2Ge_6 distorted octahedra. This distance is significantly shorter than the closest Fe-Fe distance of 2.5 Å in α-Fe, and is close to the calculated distance of 2.32 Å for a

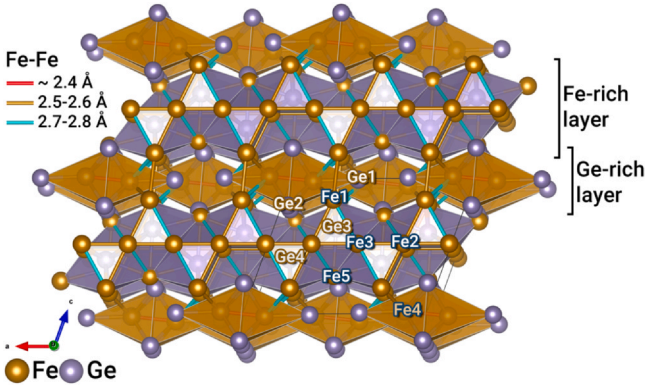

Fig. 1. Crystal structure of Fe_6Ge_5.

Fe-Fe single bond [27]. HRPD data also reveal no significant structural changes in the range of 10–373 K, while the unit cell parameters smoothly and monotonically increase with increasing temperature (Fig. 2).

3.3. Magnetic properties of Fe_6Ge_5

Fe_6Ge_5 demonstrates a very peculiar magnetic behavior that includes two antiferromagnetic phase transitions at 330 K (T_{N1}) and 110 K (T_{N2}). Temperature dependence of the magnetic susceptibility $\chi(T)$ of the Fe_6Ge_5 single crystal in various applied fields is presented in Fig. 3a,b. Above 330 K, Fe_6Ge_5 is a Curie-Weiss paramagnet (Fig. 3c). Fitting of the high-temperature magnetic susceptibility data at temperatures between 400 K and 900 K in 5 T magnetic field by the modified Curie-Weiss law yields positive Weiss temperature θ_W of 237.5(3) K and the effective moment μ_{eff} of 3.84(1) μ_B per Fe atom. These results agree well with magnetic measurements data on a Fe_6Ge_5 powder sample presented in the literature [22], which showed similar magnetic susceptibility curve, while Curie-Weiss fit yielded comparable values of θ_W and μ_{eff}.

The first transition at 330 K is clearly seen on the magnetic susceptibility curve along the b axis, while the drop of susceptibility in the ac plane is much lower. Moreover, below this transition, magnetic susceptibility along the b axis shows the pronounced field dependence, which manifests itself as S-shaped magnetization curves below 300 K (Fig. 3d). This indicates that at 330 K a significant portion of magnetic moments orders parallel to the b axis. Opposing to the first transition, the second one at 110 K has a little effect on the b axis susceptibility and does not change the shape of the magnetization curves along this axis, while dropping significantly the susceptibility in the ac plane. This implies that the second transition is associated with antiferromagnetic ordering of the ac plane components of the magnetic moments. Our HRPD data indicate no structural changes in the temperature range of 10–373 K, thus, both transitions are of purely magnetic origin.

3.4. Thermodynamic properties

Low temperature heat capacity of the Fe_6Ge_5 single crystal was measured in zero magnetic field between 2 and 125 K and in 5 T field from 100 to 125 K. Temperature dependence of heat capacity divided by temperature ($C_p(T)/T$, Fig. 4) shows a second order phase transition at 110 K both in zero field and in 5 T field. High temperature heat capacity measurements of the Fe_6Ge_5 single crystal were performed between 300 and 340 K (Fig. 4, inset) and showed another second order phase transition near 325 K. Both transitions are not only of second order, but their temperatures coincide with the temperatures taken from the magnetic susceptibility data, implying that these phase transitions are purely a result of magnetic ordering.

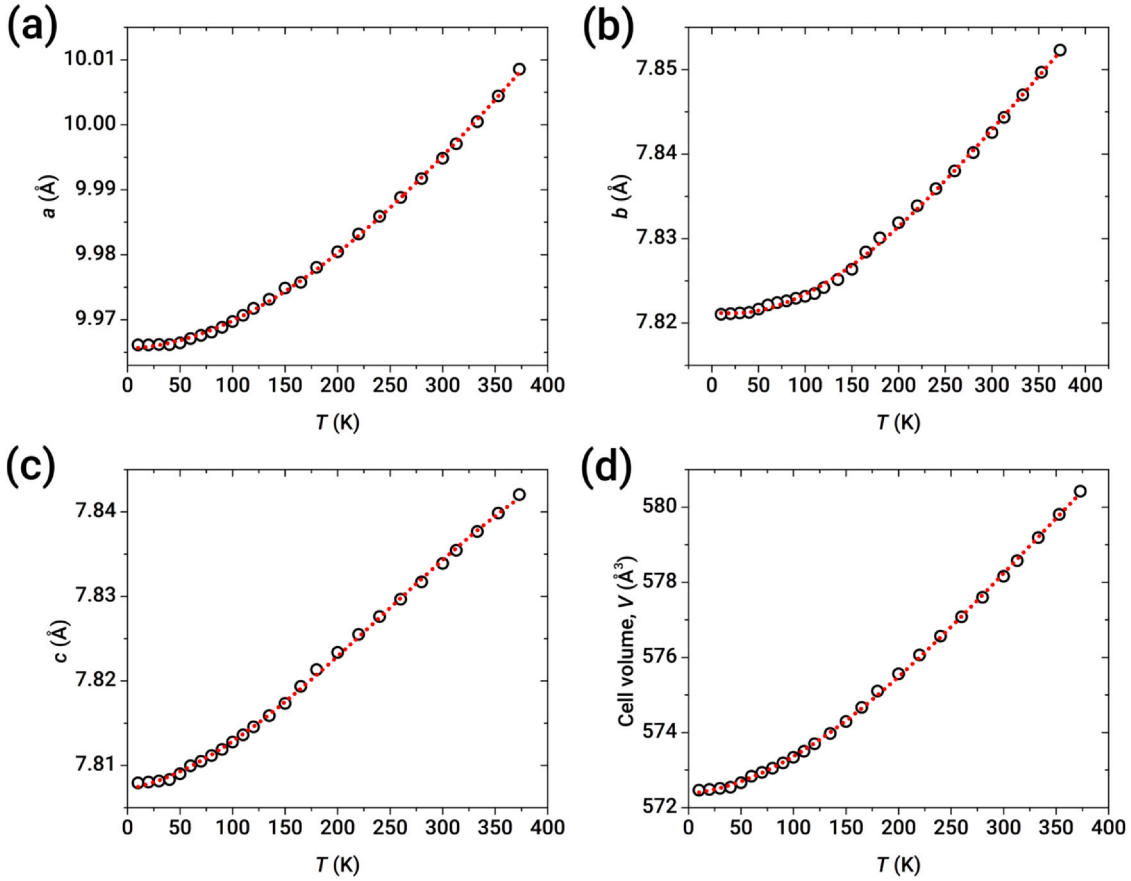

Fig. 2. Temperature dependence of the cell parameters (a–c) and cell volume (d) plotted as black dots. The red dotted curves are guides for the eye. (For interpretation of the references to colour in this figure legend, the reader is referred to the web version of this article.)

Below 20 K, heat capacity can be approximated by the equation $c_p = \gamma T + AT^3$, where γT is an electronic contribution to heat capacity and AT^3 is a sum of phononic and antiferromagnetic magnon contributions, which cannot be distinguished from each other, since they both obey the same cubic law [28,29]. The obtained value of Sommerfeld coefficient per atom, γ/atom = 5.3(2) mJ·mol^{-1}·K^{-2}, is close to that of pure iron (4.98 mJ·mol^{-1}·K^{-2} [29]), and in line with other related iron-based intermetallics that possess metallic conductivity (for instance, γ/atom = 4.42(1) mJ·mol^{-1}·K^{-2} in $Fe_{2.7}As_{0.96}Te_2$ [30]).

3.5. ^{57}Fe Mössbauer spectroscopy

The ^{57}Fe Mössbauer spectra of Fe_6Ge_5 powder were recorded in the temperature range of 14–343 K, including the points of both magnetic phase transitions at $T_{N1} \approx 330$ K and $T_{N2} \approx 110$ K. The most typical spectra of Fe_6Ge_5 in three temperature ranges are shown in Fig. 5. The best-fit hyperfine parameters and relative intensities of the subspectra for 14, 153, and 343 K are given in Table 4.

3.5.1. Paramagnetic temperature range, $T > T_{N1}$

The spectra in the paramagnetic temperature range, $T > T_{N1}$ (Fig. 5), have an asymmetric and broadened shape, which can be well described as a superposition of five quadrupole doublets Fei with an integrated intensity (A) ratio of 2:1:1:1:1, corresponding to the number and multiplicity of independent iron positions in Fe_6Ge_5. It should be noted that the assignment of each partial spectrum to a specific site in the Fe_6Ge_5 structure is not obvious. While the assignment of the most intense ($A_1 \approx 33\%$) partial spectrum is straightforward due to the different multiplicity of the Fe1 site, the assignment of the four remaining subspectra ($A_{2-5} \approx 17\%$) to specific iron sites with the same multiplicity in Fe_6Ge_5 seems less direct. In order to carry out such an analysis, we used the correlation of isomer shift (δ) and interatomic distance Fe-Ge (d_{avg}) in related iron germanides such as FeGe [4,6,11,13–15,31], $FeGe_2$ [8,24], $Fe_{32+\delta}Ge_{33}As_2$ and $Fe_{32+\delta}Ge_{35-x}P_x$ [32–34].

In earlier works [13–15] devoted to ^{57}Fe Mössbauer spectroscopy and neutron diffraction studies of the monoclinic and hexagonal modifications of FeGe, it was shown that the isomer shift of individual Fe atoms almost linearly grows with their average near-neighbor Fe-Ge distances (Fig. 6). The isomer shift of iron atoms in $FeGe_2$ [8] falls on the same line as those of hexagonal and monoclinic FeGe, while the iron atoms in cubic FeGe [31] have a significantly higher value of δ than that expected from the linear dependence. $Fe_{32+\delta}Ge_{33}As_2$ and $Fe_{32+\delta}Ge_{35-x}P_x$ that were synthesized and thoroughly studied in our previous works [32–34] also show somewhat monotonic scaling, albeit with higher values of the isomer shift (Fig. 6, the points for $Fe_{32+\delta}Ge_{35-x}P_x$ are not shown on the graph, since they are within an error from $Fe_{32+\delta}Ge_{33}As_2$). The higher values of the isomer shift in the latter cases can be associated with more covalent nature of chemical bonding, indicated by a large number of short Fe-Ge bonds (around 2.4 Å), which might cause redistribution of the electron density from the *s*-orbitals to the *p*- and *d*-orbitals of iron atoms.

Despite structural similarities to the monoclinic FeGe, the correlation between the isomer shift and interatomic distances in Fe_6Ge_5 does not follow the same monotonic dependence. The approximation with linear scaling was attempted, but yielded very poor results. The iron atoms, however, can be split into two groups with different monotonic dependencies. The first group consists of

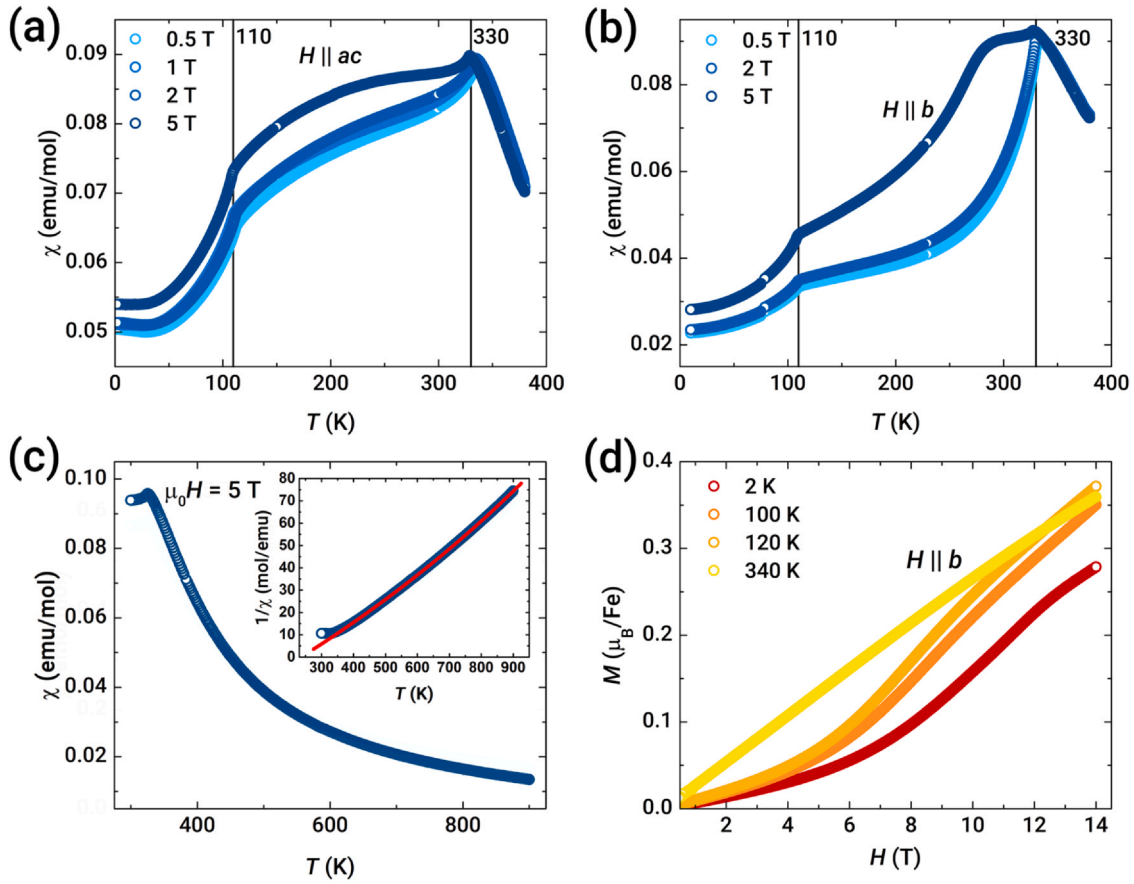

Fig. 3. Temperature dependence of the magnetic susceptibility of the Fe_6Ge_5 single crystal in various applied fields along the *ac* plane (a) and the *b* axis (b); magnetic susceptibility and reverse magnetic susceptibility (inset) of the stack of non-oriented Fe_6Ge_5 single crystals in applied field of $\mu_0H = 5$ T (c); magnetization curves of the Fe_6Ge_5 single crystal at different temperatures along the *b* axis (d). Extrapolated Curie-Weiss fit is shown on inset (c) by the red line. (For interpretation of the references to colour in this figure legend, the reader is referred to the web version of this article.)

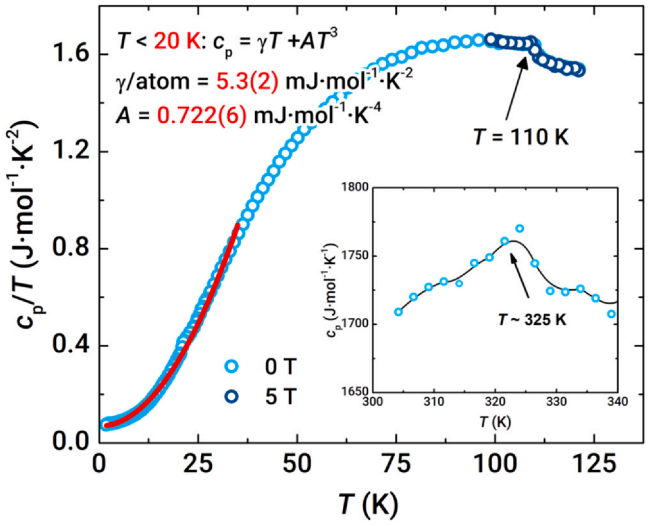

Fig. 4. Temperature dependence of heat capacity of the Fe_6Ge_5 single crystal divided by temperature (d) and heat capacity of the same crystal above 300 K (inset). Red line – extrapolated low-temperature heat capacity fit according to equation $c_p = \gamma T + AT^3$. (For interpretation of the references to colour in this figure legend, the reader is referred to the web version of this article.)

the Fe1, Fe4 and Fe5 atoms, while the second one consists of the Fe2 and Fe3 atoms (Fig. 6). The Fe2 and Fe3 atoms were chosen to be placed into a separate group, since these atoms possess similar atomic environments with the only major difference being the positions of one Fe atom and one Ge atom, which are switched (Fig. 7). While the isomer shift values for Fe2–Fe4 atoms are close, these atoms could be differentiated based on the values of hyperfine field (B_{hf}) at ^{57}Fe nuclei in the magnetically ordered region, which should be close for the Fe2 and Fe3 atoms (see the section below).

Due to the higher iron content in Fe_6Ge_5 compared to other binary germanides shown in Fig. 6, the coordination environment of individual iron sites contains a larger number of iron atoms, which also can complicate the relationship between the isomer shift and the distance to neighboring germanium atoms. It is also interesting to note that the points corresponding to the Fe2 and Fe3 atoms of Fe_6Ge_5 sit on the graph in Fig. 6 very close to the Fe4 atom in $Fe_{32+\delta}Ge_{33}As_2$. The Fe4 atom in the latter structure possesses a very similar atomic environment to that of Fe_6Ge_5 counterparts, with the differences being the partial occupation of one neighboring Fe site and the replacement of one Ge atom with the As atom (Fig. 7), which might indicate a special type of the bonding pattern for this atomic environment.

3.5.2. Magnetic "intermediate" temperature range, $T_{N2} < T < T_{N1}$

In the intermediate temperature range, $T_{N2} < T < T_{N1}$ (Fig. 5), all the spectra Fei exhibit Zeeman splitting indicating the hyperfine magnetic fields B_{hf} induced at ^{57}Fe nuclei upon the transition of the Fe_6Ge_5 crystal to the magnetically ordered state. Taking into account the results in the paramagnetic temperature range ($T > T_{N1}$), the spectra were also fitted as a superposition of five hyperfine Zeeman patterns. Due to the large number of partial spectra Fei, a number of constraints were enforced upon fitting the spectra (see the Supplementary Material). Since the maximum value of B_{hf} does not exceed ~23 T even at the lowest temperature, and the quadrupole

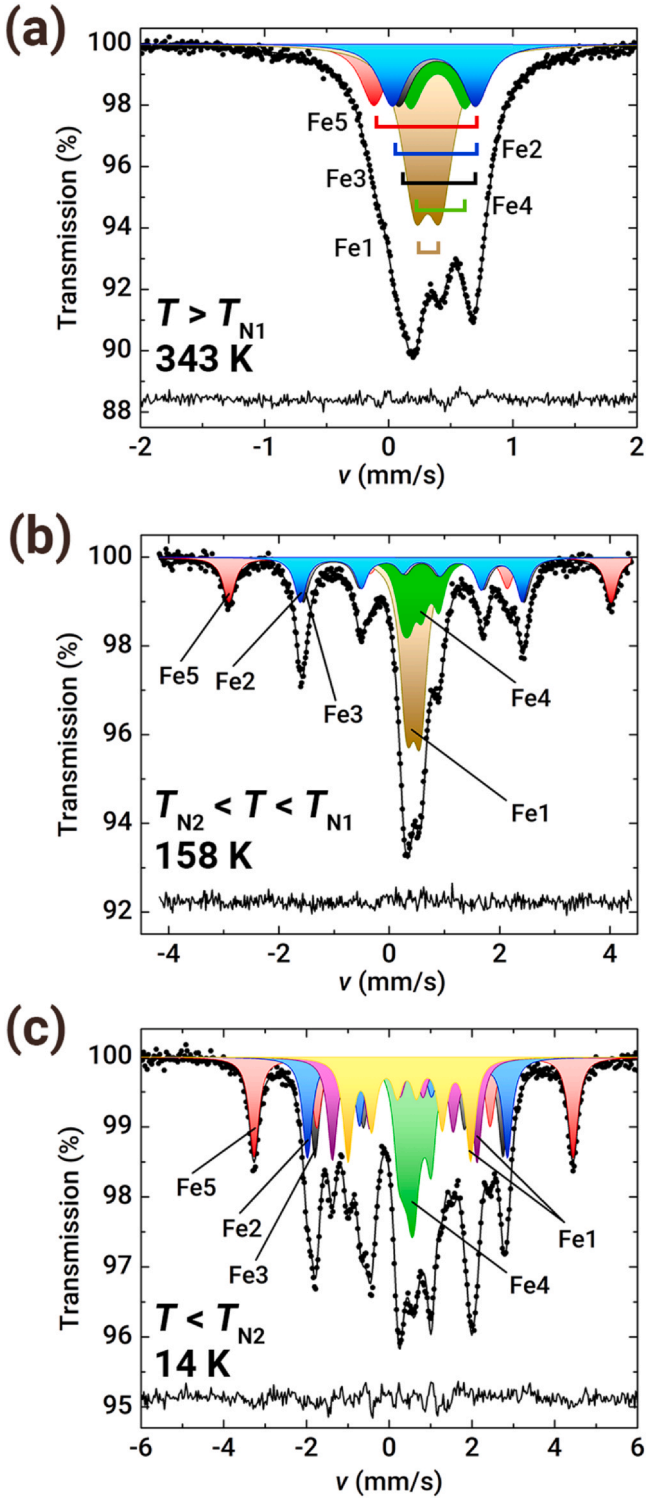

Fig. 5. Typical ^{57}Fe Mössbauer spectra of Fe_6Ge_5 in the paramagnetic region above T_{N1} (a), in the high temperature magnetic phase at $T_{N2} < T < T_{N1}$ (b) and in the low-temperature magnetic phase at $T < T_{N2}$ (c).

coupling constant reaches the values of $0.39 \le |eQV_{ZZ}| \le 1.42$ mm/s (Table 4), the spectra were analyzed by solving the full Hamiltonian $\hat{H}_{\mu Q}$ including both magnetic and quadrupole hyperfine interactions. The eigenvalues $\hat{H}_{\mu Q}$ depend not only on the hyperfine parameters (δ, eQV_{ZZ}, B_{hf}, η), but also on spherical angles (θ, φ) that determine the orientation of the hyperfine field B_{hf} in the principal axes of the electric field gradient (EFG) tensor at ^{57}Fe nuclei at different iron sites [35].

Using the above fitting model, we could satisfactorily describe the entire series of the spectra in the intermediate temperature range. The spectra exhibit Zeeman splittings, which are substantially different for different iron sites (Fig. 5). According to the B_{hf} values, iron sites can be separated into three different groups (Fig. 8). The first group consists of the Fe5 atoms, which possess the highest hyperfine fields (~23 T); the second one combines the Fe2 and Fe3 atoms with intermediate hyperfine field values (~12 T); and the third group corresponds to the Fe1 and Fe4 atoms with very low hyperfine fields (≤ 1.5 T), due to which the central part of the spectra resembles a quadrupole doublet. Such small values of B_{hf} for the latter group are likely associated not with contact Fermi interaction coming from the spin polarization of *ns*-electrons (n = 1–4) by unpaired 3*d*-electrons [36,37], but rather with the supertransferred hyperfine field contribution due to Fe-Ge-Fe superexchange [34], magnetic dipole interactions with neighboring iron atoms [38], or coupling due to the long-range interaction driven by conduction electrons [39].

3.5.3. Low-temperature range, $T < T_{N2}$

Below T_{N2}, the Mössbauer spectra significantly change (Fig. 5), mainly due to the change in the shape of the Fe1 and Fe4 partial spectra. The Fe1 partial spectrum, which in the intermediate temperature range, $T_{N2} < T < T_{N1}$, looks almost like a broadened doublet, below T_{N2} transformed into a Zeeman pattern with an average hyperfine field $< B_{hf} > \approx 10$ T (at 14 K). This fact indicates the onset of a long-range magnetic order in the Fe1 sublattice at T_{N2}. Due to the broadened and slightly asymmetrical components, the Fe1 spectrum was fitted as a distribution $p(B_{hf})$ of hyperfine fields B_{hf}, assuming a linear correlation between B_{hf} and polar angles (θ, φ) [40]. The resulting distribution $p(B_{hf})$ (Fig. 9) has a bimodal shape with two well-defined maxima B_α and B_β around 9 T and 11 T (at 14 K), respectively. The appearance of two maxima with almost equal intensities could indicate strong anisotropy of hyperfine field $B_{hf}(\theta,\varphi)$ and can be evidence for a modulated magnetic structure as was shown in our earlier works [38,41–48]. The anisotropy determined as a difference $\Delta B_{anis} = B_\beta - B_\alpha$ (Fig. 9) gradually decreases as the temperature approaches T_{N2}. Two main contributions may be responsible for the appearance of spatial anisotropy of $B_{hf}(\theta,\varphi)$: (i) the dipole contribution associated with the influence of neighbors with a nonzero magnetic moment [35]; and (ii) the contribution associated with the unquenched orbital angular momentum of iron [35]. In order to estimate the degree of "participation" of each of the contributions to the hyperfine field anisotropy for Fe1, the information on the magnetic and electronic structure of Fe_6Ge_5 is required.

Based on the above analysis of the bimodal $p(B_{hf})$ distribution, we approximated the Fe1 partial spectrum as a superposition of two subspectra Fe1α and Fe1β of the same intensity for the satisfactory further analysis of all spectra below T_{N2}. Aside from the sharp increase in B_{hf} and drastic change of polar angle θ for Fe1 at T_{N2} (Fig. 10), there is a significant change in the value of θ for the Fe4 atoms. The particularly high sensitivity of the Fe4 magnetic moment orientation to the Fe1 ordering appears to be caused by the fact that the Fe4 atom has the largest number of the nearest-neighbor Fe1 atoms. However, despite this change in the B_{hf} direction for Fe4, its absolute value is not affected by the phase transition, and does not exceed 1.5 T even at 14 K.

The average isomer shift $< \delta > = \sum_i (A_i \cdot \delta_i)$ of the experimental spectra measured in the whole temperature range gradually increases with decreasing temperature, in accordance with the Debye approximation for the second-order Doppler shift, and the best fit is achieved for the effective Debye temperature of $\Theta_D = 360(20)$ K (Fig. S3 of the Supplementary Material). This finding shows that there are

Table 4
Hyperfine parameters of the ^{57}Fe Mössbauer spectra of Fe_6Ge_5.

Temperature (K)	Site	δ (mm/s)	eQV_{zz} (mm/s)	B_{hf} (T)	W (mm/s)	A (%)
14	Fe1α	0.46(1)[a]	0.386[b]	10.82(2)	0.28(1)[a]	16.67[b]
	Fe1β	0.46(1)[a]	0.386[b]	9.12(2)	0.28(1)[a]	16.67[b]
	Fe2	0.54(1)	-1.181[b]	14.60(2)	0.28(1)[a]	16.67[b]
	Fe3	0.54(1)	1.306[b]	13.56(2)	0.28(1)[a]	16.67[b]
	Fe4	0.59(1)	0.764[b]	1.39(2)	0.28(1)[a]	16.67[b]
	Fe5	0.47(1)	1.418[b]	23.36(2)	0.28(1)[a]	16.67[b]
153	Fe1	0.44(1)	0.386[b]	0.54(3)	0.27(1)[a]	33.33[b]
	Fe2	0.52(1)	-1.181[b]	11.93(5)	0.27(1)[a]	16.67[b]
	Fe3	0.49(1)	1.306[b]	11.94(5)	0.27(1)[a]	16.67[b]
	Fe4	0.52(1)	0.764[b]	1.05(3)	0.27(1)[a]	16.67[b]
	Fe5	0.42(1)	1.418[b]	20.90(3)	0.27(1)[a]	16.67[b]
343	Fe1	0.315(2)	0.386(7)	–	0.256(3)[a]	33.33[b]
	Fe2	0.391(5)	-1.181(4)	–	0.256(3)[a]	16.67[b]
	Fe3	0.365(4)	1.306(3)	–	0.256(3)[a]	16.67[b]
	Fe4	0.397(5)	0.764(15)	–	0.256(3)[a]	16.67[b]
	Fe5	0.291(2)	1.418(4)	–	0.256(3)[a]	16.67[b]

[a] these values are constrained.
[b] these values are fixed.

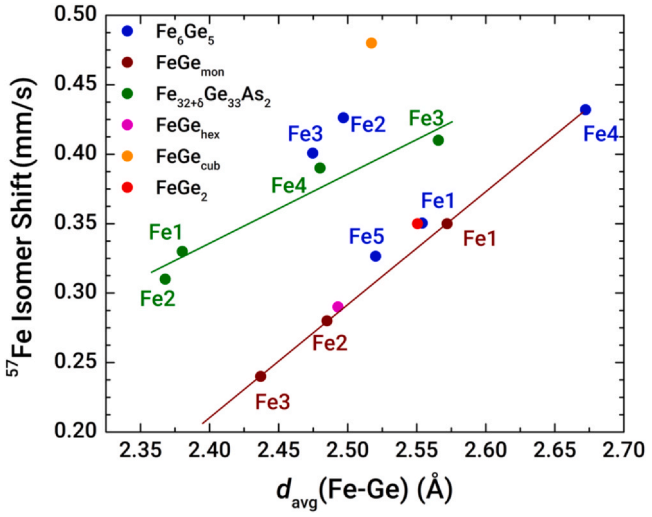

Fig. 6. Isomer shift at ambient temperature for individual Fe sites in Fe_6Ge_5 and related compounds plotted against the average Fe-Ge distance (d_{avg}) for each site. The data points for other iron germanides are taken from the literature [4,6,8,11,13–15,26,31–34].

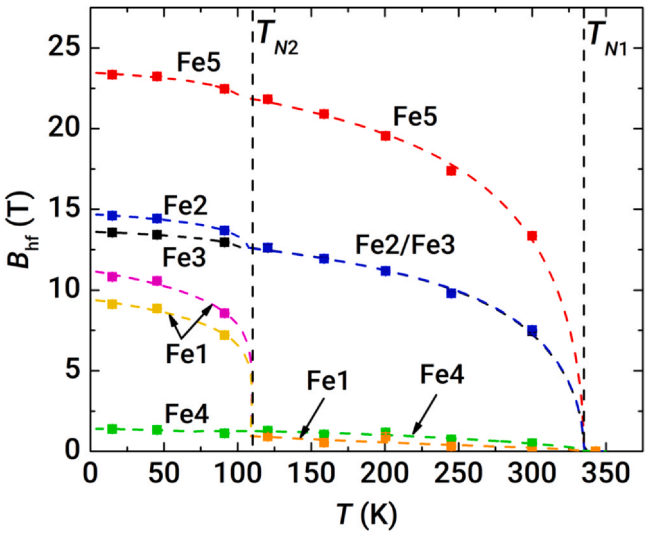

Fig. 8. Temperature dependencies of the hyperfine magnetic fields at ^{57}Fe nuclei.

no electronic or structural phase transitions at low temperatures. Just below T_{N1} and T_{N2}, the hyperfine fields $B_{hf}(T)$ of all partial subspectra increase smoothly with decreasing temperature (Fig. 8), following the temperature dependence of the magnetizations in iron sublattices, and thus underlying the second-order nature of the magnetic phase transitions.

4. Discussion

The crystal structure of Fe_6Ge_5 is closely related to the crystal structures of many phases in the Fe-Ge system, most notably β-$Fe_{2-\delta}Ge$, η-$Fe_{7-\delta}Ge_4$, and the monoclinic modification of FeGe [1,13,25]. As can be seen in Fig. 11, all these compounds also feature similar zig-zag layers of germanium-centered trigonal prisms. Such a

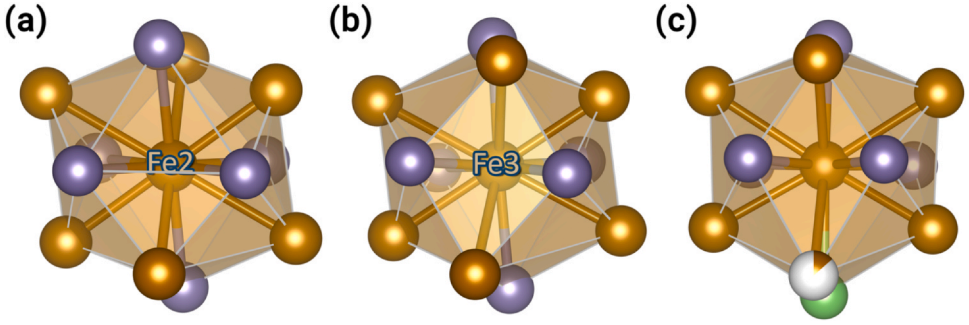

Fig. 7. Coordination polyhedra for Fe2 and Fe3 atoms in Fe_6Ge_5 (a and b respectively), and Fe4 in $Fe_{32+\delta}Ge_{33}As_2$ (c) [32].

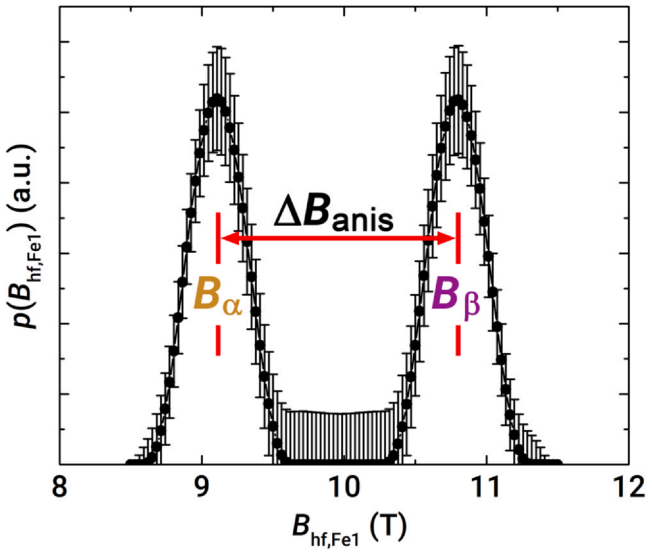

Fig. 9. Hyperfine field distribution $p(B_{hf})$ at the Fe1 site.

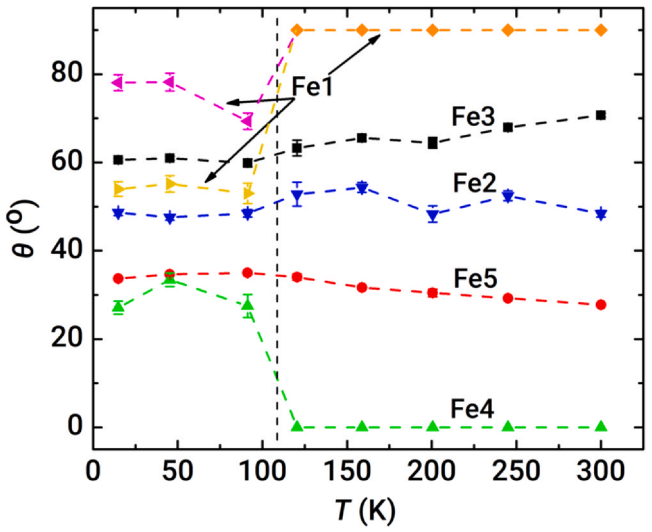

Fig. 10. Temperature dependencies of the polar angle θ of the hyperfine field for Fe atoms in Fe_6Ge_5.

trigonal-prismatic environment of *p*-element atoms is very common amongst transition metal tetrelides, with the Fe-Ge compounds being the case example of it. Phases in the Fe-Ge system are built primarily from the derivatives of a 5-capped trigonal prism of Fe atoms surrounding a Ge atom, which is observed in β-$Fe_{2-\delta}Ge$ [1,25]. Upon transition to the Ge-rich region, the 11-vertex polyhedron

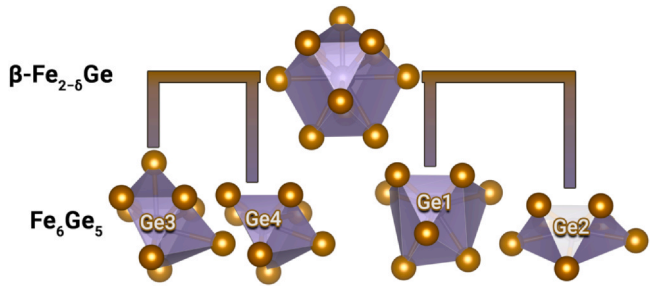

Fig. 12. The evolution of Ge polyhedron from the β-phase in Fe-Ge system to Fe_6Ge_5.

loses its vertices leading to gaps and abruptions in the Fe framework and to its reduced dimensionality [1]. The topology of this framework defines magnetic properties of compounds in the Fe-Ge system due to a competition between the ferromagnetic Fe-Fe direct exchange and antiferromagnetic Fe-Ge-Fe superexchange interactions [1].

The crystal structure of Fe_6Ge_5 contains 4 different Ge polyhedra, the shape of which can be traced back to the 5-capped trigonal prism $GeFe_{11}$ in β-$Fe_{2-\delta}Ge$. The transformation of the initial $GeFe_{11}$ polyhedron into the polyhedra featured in Fe_6Ge_5 requires removing 2 or 4 iron atoms at the vertices and a slight distortion of the polyhedron as can be seen in Fig. 12. While iron atoms in the initial $GeFe_{11}$ polyhedron form a uniform cage with short 2.5–2.6 Å contacts between Fe atoms, each Ge polyhedron, in Fe_6Ge_5, as a result of losing some vertices, features several short (2.5–2.8 Å) and long (around 4 Å) Fe-Fe distances on the edges. This leads to gaps in the 3-dimensional Fe framework making it less bound in comparison to the ferromagnetic β-$Fe_{2-\delta}Ge$ (Fig. 13a and b) and η- $Fe_{7-\delta}Ge_4$ (Fig. 13c and d). The entire iron skeleton can be divided in fragments of lower dimensionality that are sewn together by several short Fe-Fe contacts. In addition to the mentioned above layers alternating in the *c* direction, one can distinguish separate Fe layers along the *ac* plane or the (2 0 1) plane that are connected by a comparable number of Ge and Fe atoms (Fig. 13e and f).

Thus, the Fe framework in Fe_6Ge_5 can be considered as intermediate between clearly 3-dimensional networks of short Fe-Fe contacts in β- and η-phases and Fe networks of lower dimensionality such as one presented in the hexagonal polymorph of FeGe (Fig. 13). A similar, but less bound Fe framework is present in the monoclinic modification of FeGe (Fig. 13g), which also possesses a formally 3-dimensional Fe framework that can be divided into smaller loosely connected fragments.

The similarities in the iron frameworks of Fe_6Ge_5 and $FeGe_{mon}$ are translated into their magnetic properties. Both compounds are antiferromagnets and undergo two magnetic phase transitions, with their temperatures differing by only 10 K between the phases. T_{N1} and T_{N2} of Fe_6Ge_5 are 330 K and 110 K respectively, while monoclinic FeGe experience transitions at 340 K and 120 K [12–15]. Despite their

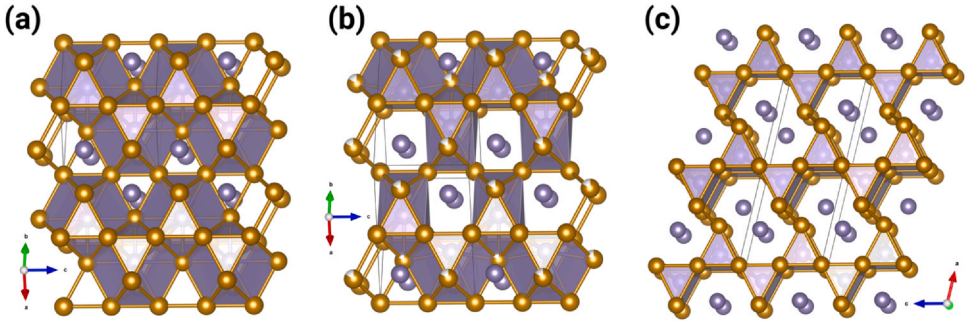

Fig. 11. Crystal structures of β-$Fe_{2-\delta}Ge$ (a), η-$Fe_{7-\delta}Ge_4$ (b), and the monoclinic modification of FeGe (c) [13,25].

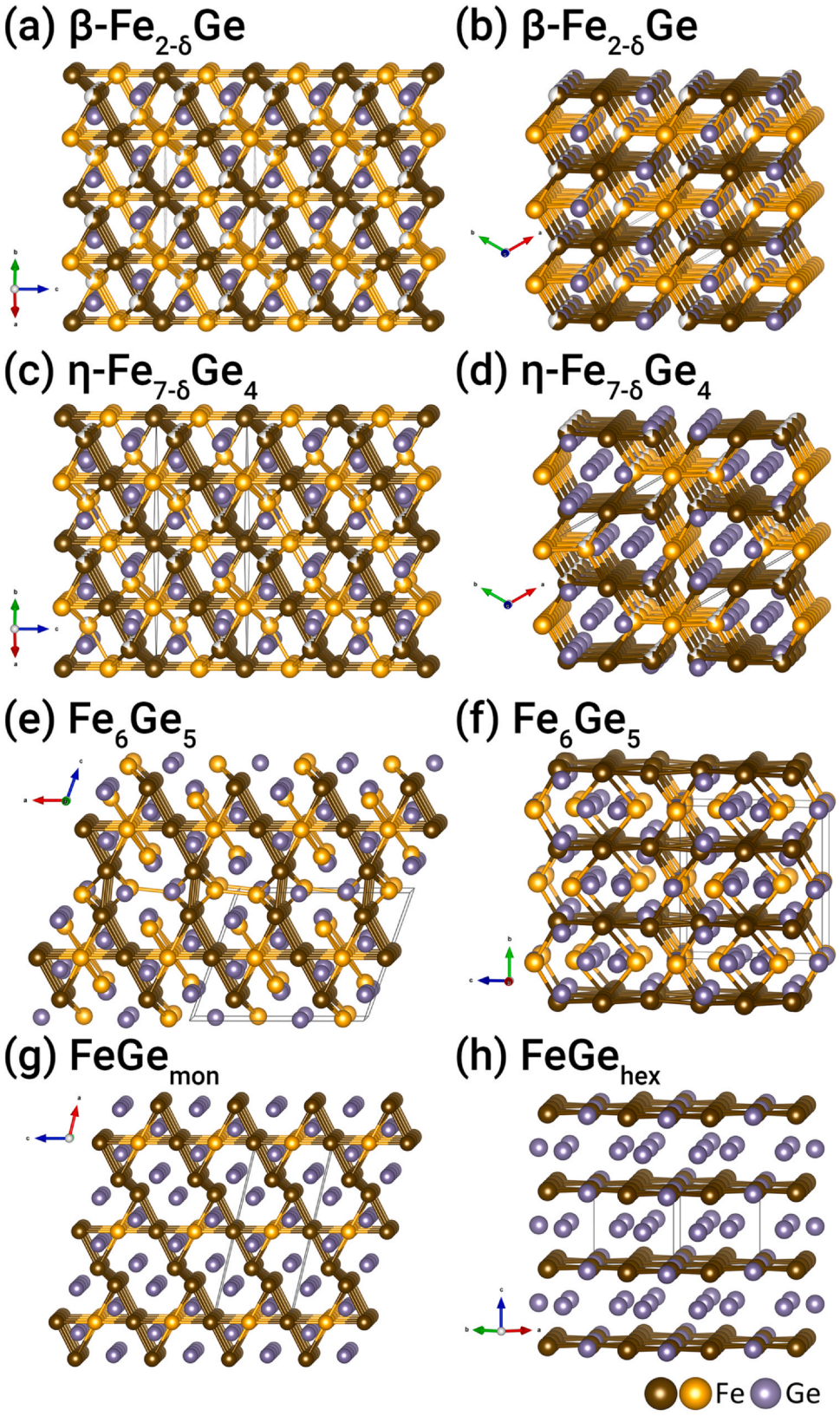

Fig. 13. Comparison of the iron frameworks in the crystal structures of β-$Fe_{2-\delta}Ge$ (a,b), η-$Fe_{7-\delta}Ge_4$ (c,d) [25], Fe_6Ge_5 (e,f), $FeGe_{mon}$ (g) [13] and $FeGe_{hex}$ (h) [4]. Iron atoms are shown in different colors to highlight dissections of the structures into layers.

antiferromagnetic ordering, both compounds possess positive Weiss temperatures, which indicates strong ferromagnetic interactions and underlines the intricate nature of magnetism in them originating from the complex and sparsely connected frameworks of Fe atoms and a competition between ferromagnetic and antiferromagnetic couplings.

It is interesting to note that while the magnetic susceptibility of FeGe demonstrates an increase at intermediate temperatures, the

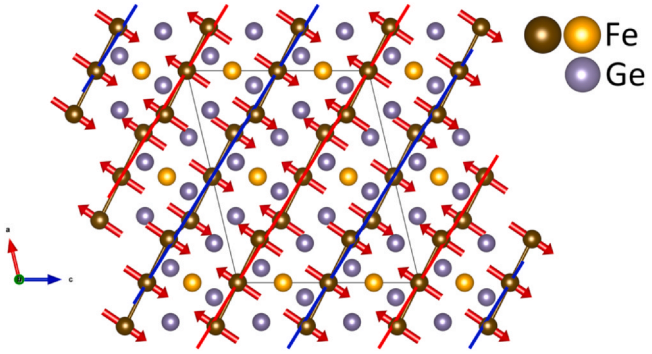

Fig. 14. Layered (+ −) antiferromagnetic ordering in monoclinic FeGe between 120 and 340 K [12–15].

magnetic susceptibility of Fe_6Ge_5 only decreases below the high-temperature magnetic transition, implying that disordered magnetic moments are either strongly coupled or heavily influenced by the ordered spins. A somewhat similar deviation from the Curie-Weiss behavior we have recently observed in another related iron germanide – $Fe_{32+\delta}Ge_{33}As_2$ [32].

Despite the absence of the magnetic susceptibility upturn between T_{N2} and T_{N1}, the described above temperature evolution of hyperfine fields (Fig. 8) clearly shows that magnetic moments of at least Fe1 atoms do not experience long range ordering in this temperature region. Given that B_{hf} at the Fe4 nuclei remains small even at low temperatures, the cause of the lack of noticeable ordered magnetic moments at these atoms is less clear. Such consistently small values of hyperfine field for Fe4 atoms could be associated with low intrinsic magnetic moments on these atoms or with disordered spins of Fe4 atoms, which are strongly antiferromagnetically coupled. Such small values of ordered magnetic moments are not common amongst metallic iron germanides; however, in our previous work [34], we observed in $Fe_{32+\delta}Ge_{33}As_2$ small values of B_{hf} ≈ 2.5 T associated with small magnetic moments of ~0.25 μ_B per atom.

Such behavior in the intermediate temperature range $T_{N2} < T < T_{N1}$, known as a partially disordered (PD) state, has been found for some systems with competing exchange interactions [49,50] as well as in monoclinic FeGe [12–15]. In the latter, unlike Fe_6Ge_5, the magnetic hyperfine fields on iron atoms that are not involved in ordering seem to be negligible, since their Mössbauer subspectra were approximated only as quadrupole doublets [12–15].

Combining our magnetic susceptibility and ^{57}Fe Mössbauer spectroscopy data, the following scheme of magnetic ordering in Fe_6Ge_5 can be established. The high temperature magnetic transition mainly involves the Fe2, Fe3, and Fe5 sites, in which iron atoms order their magnetic moments along the *b* axis in an antiferromagnetic fashion. The low-temperature transition at T_{N2} causes antiferromagnetic ordering of magnetic moments of the Fe1 atoms within the *ac* plane, while other iron atoms mostly conserve values and orientations of their magnetic moments.

The origin of the partially disordered state in monoclinic FeGe lies in hidden geometric frustration in the crystal structure, which is revealed upon the first antiferromagnetic transition that creates a layered (+ −) antiferromagnetic structure [12–15] (Fig. 14). The nearest-neighbor Fe1 and Fe2 atoms order ferromagnetically creating layers parallel to the (1 0 1/2) plane with the layers themselves coupling antiferromagnetically. This ordering causes frustration for the magnetic moment on the Fe3 site, since there is no preferred orientation for the moment. This frustration resolves only at 120 K creating a complex modulated pattern [12–15].

A similar picture can be proposed in the case of Fe_6Ge_5: The adjacent Fe2, Fe3, and Fe5 atoms create ferromagnetically coupled layers (Fig. 15) that order antiferromagnetically in a layered (+ −) fashion with respect to each other at T_{N1}. This creates magnetic frustration on the Fe1 and Fe4 sites between the layers, which are related by the center of inversion and nearly mirror each other. This frustration resolves only at low temperatures creating a supposedly modulated structure due to magnetic ordering of the Fe1 atoms.

5. Conclusions

Our study of Fe_6Ge_5 presents a detailed view on the crystal structure of this compound as well as a comprehensive analysis of the magnetic behavior and its origin with the help of the magnetization measurements and ^{57}Fe Mössbauer spectroscopy study. Our model of the crystal structure is generally consistent with the model presented in the literature [18], while provides more uniform values of atomic displacement parameters expected for such a closely packed structure without large voids. The crystal structure of Fe_6Ge_5 is complex with 5 independent Fe sites and 4 Ge sites and resembles both high-temperature modifications of FeGe and iron-rich phases such as β-$Fe_{2-\delta}Ge$ and η-$Fe_{7-\delta}Ge_4$. These structure relationships are also reflected in the framework of iron atoms in Fe_6Ge_5 that has similarities with monoclinic FeGe and also can be considered intermediate between three-dimensional iron frameworks in iron-rich phases and two-dimensional separated iron layers of hexagonal FeGe. While the Fe framework in Fe_6Ge_5 is more complex and does feature more such Fe-Fe interconnections, the magnetic behavior of Fe_6Ge_5 and monoclinic FeGe is still very similar. Both phases are antiferromagnetic, and the magnetic ordering occurs in two steps with similar temperatures of phase transitions, 110 and 330 K for Fe_6Ge_5 versus 120 and 340 K for monoclinic FeGe. The ^{57}Fe Mössbauer spectroscopy study of Fe_6Ge_5 reveals that each transition mainly affects different iron sites with a possible formation of a modulated magnetic structure at low temperatures, which is again similar to monoclinic FeGe. Such magnetic behavior in both cases originates from competing ferromagnetic near-neighbor exchange and antiferromagnetic superexchange interactions and the underlying frustration hidden in the crystal structure of both compounds.

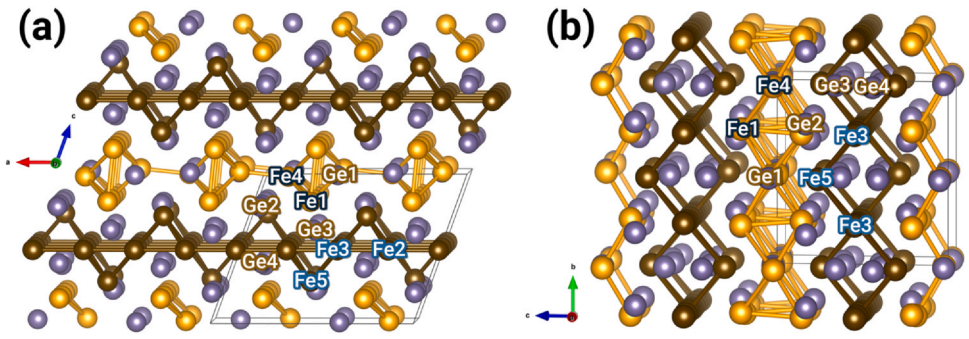

Fig. 15. Proposed splitting of iron atoms in Fe_6Ge_5 into two groups (marked by different colors) that results in magnetic frustration on the Fe1 site.

CRediT authorship contribution statement

Roman A. Khalaniya: Conceptualization, Methodology, Investigation, Visualization, Validation, Formal analysis, Data curation, Writing – original draft, Writing – review & editing. **Valeriy Yu. Verchenko:** Investigation, Validation, Formal analysis, Writing – review & editing, Funding acquisition. **Alexey V. Sobolev:** Investigation, Validation, Formal analysis, Writing – original draft, Writing – review & editing. **Igor A. Presniakov:** Investigation, Validation, Writing – review & editing. **Zheng Wei:** Investigation, Validation. **Evgeny V. Dikarev:** Writing – review & editing, Funding acquisition. **Andrei V. Shevelkov:** Conceptualization, Writing – review & editing, Supervision, Funding acquisition.

Declaration of Competing Interest

The authors declare that they have no known competing financial interests or personal relationships that could have appeared to influence the work reported in this paper.

Acknowledgements

This work has been supported by the Russian Science Foundation, grant № 17–13-01033. The authors acknowledge the European Synchrotron Radiation Facility (ESRF, Grenoble, France) for granting the beam time and thank Dr. Wilson Mogodi for his help during the high-resolution powder X-ray diffraction experiments under the proposal HC-3841. V.Yu.V. appreciates the support from the European Regional Development Fund and Mobilitas Program, grant no. MOBJD449. The single-crystal study at UAlbany has been funded by the National Science Foundation, grant No. CHE-1955585.

Appendix A. Supporting information

Supplementary data associated with this article can be found in the online version at doi:10.1016/j.jallcom.2022.163759.

References

[1] R.A. Khalaniya, A.V. Shevelkov, When two is enough: on the origin of diverse crystal structures and physical properties in the Fe-Ge system, J. Solid State Chem. 270 (2019) 118–128, https://doi.org/10.1016/j.jssc.2018.10.030
[2] H. Okamoto, Fe-Ge (iron-germanium), 292–292, J. Phase Equil. Diff. 29 (3) (2008), https://doi.org/10.1007/s11669-008-9309-9
[3] V.Y. Verchenko, Z. Wei, A.A. Tsirlin, C. Callaert, A. Jesche, J. Hadermann, E.V. Dikarev, A.V. Shevelkov, Crystal growth of the Nowotny chimney ladder phase Fe_2Ge_3: exploring new Fe-based narrow-gap semiconductor with promising thermoelectric performance, Chem. Mater. 29 (23) (2017) 9954–9963, https://doi.org/10.1021/acs.chemmater.7b03300
[4] K. Kanematsu, T. Ohoyama, Magnetic and X-ray studies of iron-germanium system II. Phase diagram and magnetism of each phase, J. Phys. Soc. Jpn. 20 (2) (1965) 236–242, https://doi.org/10.1143/JPSJ.20.236
[5] T. Ericsson, W. Karner, L. Häggström, K. Chandra, Magnetic structure of cubic FeGe, Phys. Scr. 23 (6) (1981) 1118, https://doi.org/10.1088/0031-8949/23/6/015
[6] B. Lebech, J. Bernhard, T. Freltoft, Magnetic structures of cubic FeGe studied by small–angle neutron scattering, J. Phys.: Condens. Matter 1 (35) (1989) 6105, https://doi.org/10.1088/0953-8984/1/35/010
[7] H. Wilhelm, M. Baenitz, M. Schmidt, U.K. Rößler, A.A. Leonov, A.N. Bogdanov, Precursor phenomena at the magnetic ordering of the cubic helimagnet FeGe, Phys. Rev. Lett. 107 (12) (2011) 127203, https://doi.org/10.1103/PhysRevLett.107.127203
[8] J.B. Forsyth, C.E. Johnson, P.J. Brown, The magnetic structure and hyperfine field of $FeGe_2$, Philos. Mag. 10 (106) (1964) 713–721, https://doi.org/10.1080/14786436408228489
[9] J.B. Forsyth, C. Wilkinson, P. Gardner, The low-temperature magnetic structure of hexagonal FeGe, J. Phys. F: Met. Phys. 8 (10) (1978) 2195, https://doi.org/10.1088/0305-4608/8/10/019
[10] J. Bernhard, B. Lebech, O. Beckman, Neutron diffraction studies of the low–temperature magnetic structure of hexagonal FeGe, J. Phys. F: Met. Phys. 14 (1984) 2379, https://doi.org/10.1088/0305-4608/14/10/017
[11] L. Häggström, T. Ericsson, R. Wäppling, E. Karlsson, Mössbauer study of hexagonal FeGe, Phys. Scr. 11 (1) (1975) 55–59, https://doi.org/10.1088/0031-8949/11/1/009
[12] R. Wäppling, L. Häggström, E. Karlsson, Magnetic properties of FeGe studied by Mössbauer effect, Phys. Scr. 2 (4–5) (1970) 233, https://doi.org/10.1088/0031-8949/2/4-5/018
[13] G.P. Felcher, J.D. Jorgensen, Magnetic structures of monoclinic FeGe, J. Phys. C: Solid State Phys. 16 (32) (1983) 6281, https://doi.org/10.1088/0022-3719/16/32/018
[14] D. Fruchart, B. Malaman, G. Le Caer, B. Roques, Structures magnétiques de FeGe monoclinique, Phys. Status Solidi A 78 (1983) 555–569, https://doi.org/10.1002/pssa.2210780222
[15] C. Max, G. Le Caer, B. Roques, Etude des propriétés magnétiques de la variété monoclinique du monogermaniure de fer, J. Solid State Chem. 14 (2) (1975) 172–180, https://doi.org/10.1016/0022-4596(75)90008-0
[16] C.P. Adams, T.E. Mason, S.A.M. Mentink, E. Fawcett, The magnetic phase diagram and transport properties of $FeGe_2$, J. Phys.: Condens. Matter 9 (1997) 1347, https://doi.org/10.1088/0953-8984/9/6/018
[17] T.E. Mason, C.P. Adams, S.A.M. Mentink, E. Fawcett, A.Z. Menshikov, C.D. Frost, J.B. Forsyth, T.G. Perring, T.M. Holden, Itinerant antiferromagnetism in $FeGe_2$, Phys. B 237–238 (1997) 449–452, https://doi.org/10.1016/S0921-4526(97)00128-2
[18] B. Malaman, M.J. Philippe, B. Roques, A. Courtois, J. Protas, Structures cristallines des phases Fe_6Ge_5 et Fe_6Ga_5, Acta Crystallogr., Sect. B: Struct. Crystallogr. Cryst. Chem. 30 (9) (1974) 2081–2087, https://doi.org/10.1107/S0567740874006522
[19] A.K. Larsson, S. Furuseth, R. Withers, On the crystal structure of Fe_6Ge_5 and its relationship to B8-type structures, J. Solid State Chem. 141 (1) (1998) 199–204, https://doi.org/10.1006/jssc.1998.7951
[20] J.N. Hausmann, R.A. Khalaniya, C. Das, I. Remy-Speckmann, S. Berendts, A.V. Shevelkov, P.W. Menezes, Intermetallic Fe_6Ge_5 formation and decay of a core-shell structure during the oxygen evolution reaction, Chem. Comm. 57 (17) (2021) 2184–2187, https://doi.org/10.1039/D0CC08035G
[21] K. Kanematsu, Magnetic and X-Ray studies of iron-germanium system I. Partial diagram of phase with $B8_2$ and its variant type of structure, J. Phys. Soc. Jpn. 20 (1) (1965) 36–43, https://doi.org/10.1143/JPSJ.20.36
[22] B. Malaman, A. Courtois, J. Protas, B. Roques, Propriétés magnétiques des germaniures Fe_6Ge_5-χ et FeGe monoclinique, C. R. Seances Acad. Sci., Ser. B 276 (1973) 323–326.
[23] V. Petricek, M. Dusek, L. Palatinus, Crystallographic computing system JANA2006: general features, Z. für Krist. – Cryst. Mater. 229 (2014) 345–352, https://doi.org/10.1515/zkri-2014-1737
[24] M.E. Matsnev, V.S. Rusakov, SpectrRelax: an application for Mössbauer spectra modeling and fitting, AIP Conf. Proc. 1489 (2012) 178–185, https://doi.org/10.1063/1.4759488
[25] B. Malaman, J. Steinmetz, B. Roques, Étude structurale des germaniures Fe$(Co)_{2-x}$Ge de type β et η, et de leurs alliages avec le gallium Fe$(Co)_{2-x}Ge_{1-y}Ga_y$, J. Less–Common Met. 75 (2) (1980) 155–176, https://doi.org/10.1016/0022-5088(80)90114-9
[26] E.E. Havinga, H. Damsma, P. Hokkeling, Compounds and pseudo-binary alloys with the $CuAl_2$(C16)-type structure I. Preparation and X-ray results, J. Less-Common Met 27 (2) (1972) 169–186, https://doi.org/10.1016/0022-5088(72)90028-8
[27] P. Pyykkö, M. Atsumi, Molecular single-bond covalent radii for elements 1–118, Chem. – Eur. J. 15 (1) (2009) 186–197, https://doi.org/10.1002/chem.200800987
[28] C. Kittel, Quantum Theory of Solids, 2 ed..., Wiley, New York, 1987, pp. 58–63.
[29] C. Kittel, Introduction to Solid State Physics, 8 ed..., Wiley, New York, 2005, pp. 145–146.
[30] V. Yu Verchenko, S.A. Sokolov, A.A. Tsirlin, A.V. Sobolev, I.A. Presniakov, M.A. Bykov, M.A. Kirsanova, A.V. Shevelkov, New Fe-based layered telluride $Fe_{3-\delta}As_{1-y}Te_2$: synthesis, crystal structure and physical properties, Dalton Trans. 45 (42) (2016) 16938–16947, https://doi.org/10.1039/C6DT02721K
[31] R. Wäppling, L. Häggström, Mössbauer study of cubic FeGe, Phys. Lett. A 28 (3) (1968) 173–174, https://doi.org/10.1016/0375-9601(68)90183-7
[32] R.A. Khalaniya, A.V. Mironov, V.Yu Verchenko, A. Jesche, A.A. Tsirlin, A.V. Shevelkov, Nontrivial recurrent intergrowth structure and unusual magnetic behavior of intermetallic compound $Fe_{32+\delta}Ge_{33}As_2$, Inorg. Chem. 55 (24) (2016) 12953–12961, https://doi.org/10.1021/acs.inorgchem.6b02412
[33] R.A. Khalaniya, V.Yu Verchenko, Z. Wei, E.V. Dikarev, I. Heinmaa, R. Stern, A. Jesche, A.A. Tsirlin, A.V. Shevelkov, From $Fe_{32+\delta}Ge_{35-x}P_x$ to $Fe_{32+\delta}Ge_{35-x-y}P_xAs_y$: fine geometry optimization in new intergrowth structures, J. Alloy. Compd. 779 (2019) 229–236, https://doi.org/10.1016/j.jallcom.2018.11.208
[34] R.A. Khalaniya, A.V. Sobolev, V.Yu Verchenko, A.A. Tsirlin, A. Senyshyn, F. Damay, I.A. Presniakov, A.V. Shevelkov, Magnetic structures of $Fe_{32+\delta}Ge_{33}As_2$ and $Fe_{32+\delta'}Ge_{35-x}P_x$ intermetallic compounds: a neutron diffraction and 57 Fe Mössbauer spectroscopy study, Dalton Trans. 50 (6) (2021) 2210–2220, https://doi.org/10.1039/D0DT03923C
[35] P. Gütlich, E. Bill, A.X. Trautwein, Mössbauer spectroscopy and transition metal chemistry: fundamentals and applications, Springer-Verlag, Berlin-Heidelberg, 2012.
[36] B.C. Tofield, Covalency effects in magnetic interactions, J. Phys., Colloq. 37 (C6) (1976) C6-539–C6-570, https://doi.org/10.1051/jphyscol:19766115
[37] P. Berastegui, S.G. Eriksson, S. Hull, A neutron diffraction study of the temperature dependence of $Ca_2Fe_2O_5$, Mater. Res. Bull. 34 (2) (1999) 303–314, https://doi.org/10.1016/S0025-5408(99)00007-0
[38] A.V. Sobolev, I.A. Presniakov, A.A. Gippius, I.V. Chernyavskii, M. Schaedler, N. Buettgen, S.A. Ibragimov, I.V. Morozov, A.V. Shevelkov, Helical magnetic structure and hyperfine interactions in FeP studied by ^{57}Fe Mössbauer spectroscopy and ^{31}P NMR, J. Alloy. Compd. 675 (2016) 277–285, https://doi.org/10.1016/j.jallcom.2016.03.123

[39] P. Bruno, Theory of intrinsic and thermally induced interlayer magnetic coupling between ferromagnetic films separated by an insulating layer, Phys. Rev. B 49 (18) (1994) 13231–13234, https://doi.org/10.1103/PhysRevB.49.13231
[40] M.E. Matsnev, V.S. Rusakov, Study of spatial spin-modulated structures by Mössbauer spectroscopy using SpectrRelax, AIP Conf. Proc. 1622 (1) (2014) 40–49.
[41] A.A. Aslandukova, A.V. Sobolev, I.G. Silkin, I.V. Morozov, I.S. Glazkova, I.A. Presniakov, ^{57}Fe probe Mössbauer study of magnetic phase transitions in MnP phosphide, J. Exp. Theor. Phys. 130 (6) (2020) 864–872, https://doi.org/10.1134/S1063776120050027
[42] I.S. Glazkova, A.A. Belik, A.V. Sobolev, M.N. Smirnova, N.S. Ovanesyan, I.A. Presniakov, Modulated magnetic structures in $BaRFeO_4$ (R= Y and Dy): Magnetic and ^{57}Fe Mössbauer investigations, J. Phys. Chem. C. 124 (24) (2020) 13374–13384, https://doi.org/10.1021/acs.jpcc.0c03506
[43] A.V. Sobolev, V.S. Rusakov, A.M. Gapochka, I.S. Glazkova, T.V. Gubaidulina, M.E. Matsnev, A.A. Belik, I.A. Presniakov, ^{57}Fe Mössbauer spectroscopy study of cycloidal spin arrangements and magnetic transitions in $BiFe_{1-x}Co_xO_3$, Phys. Rev. B 101 (22) (2020) 224409, https://doi.org/10.1103/PhysRevB.101.224409
[44] A.V. Sobolev, A.A. Akulenko, I.S. Glazkova, E.A. Zvereva, N.S. Ovanesyan, M.M. Markina, I.A. Presniakov, Spin ordering and hyperfine interactions in langasite-like ferrite $Ba_3SbFe_3Si_2O_{14}$: ^{57}Fe Mössbauer reinvestigation and ESR measurements, J. Alloy. Compd. 797 (2019) 432–442, https://doi.org/10.1016/j.jallcom.2019.05.020
[45] A.V. Sobolev, A.A. Akulenko, I.S. Glazkova, A.A. Belik, T. Furubayashi, L.V. Shvanskaya, O.V. Dimitrova, I.A. Presniakov, Magnetic hyperfine interactions in the mixed-valence compound $Fe_7(PO_4)_6$ from Mössbauer Experiments, J. Phys. Chem. C. 122 (34) (2018) 19767–19776, https://doi.org/10.1021/acs.jpcc.8b05516
[46] A.V. Sobolev, A.A. Akulenko, I.S. Glazkova, D.A. Pankratov, I.A. Presniakov, Modulated magnetic structure of Fe_3PO_7 as seen by ^{57}Fe Mössbauer spectroscopy, Phys. Rev. B. 97 (10) (2018) 104415, https://doi.org/10.1103/physrevb.97.104415
[47] A. Sobolev, V. Rusakov, A. Moskvin, A. Gapochka, A. Belik, I. Glazkova, A. Akulenko, G. Demazeau, I. Presniakov, ^{57}Fe Mössbauer study of unusual magnetic structure of multiferroic 3R-$AgFeO_2$, J. Phys.: Condens. Matter 29 (27) (2017) 275803, https://doi.org/10.1088/1361-648X/aa70ae
[48] A.V. Sobolev, I.A. Presnyakov, V.S. Rusakov, A.M. Gapochka, Y.S. Glazkova, M.E. Matsnev, D.A. Pankratov, Mössbauer study of the modulated magnetic structure of $FeVO_4$, J. Exp. Theor. Phys. 124 (6) (2017) 943–956, https://doi.org/10.1134/S1063776117060164
[49] M. Mekata, Antiferro-ferrimagnetic transition in triangular Ising lattice, J. Phys. Soc. Jpn. 42 (1) (1977) 76–82, https://doi.org/10.1103/PhysRevB.49.13231
[50] S. Fujiki, K. Shutoh, S. Katsura, Possibility of the Kosterlitz-Thouless phase transition in the two dimensional fully frustrated Ising model, J. Phys. Soc. Jpn. 53 (4) (1984) 1371–1379, https://doi.org/10.1143/JPSJ.53.1371